

The surface climatology of an ordinary katabatic wind regime in Coats Land, Antarctica

By IAN A. RENFREW* and PHILIP S. ANDERSON, *British Antarctic Survey, High Cross, Madingley Rd, Cambridge CB3 0ET, UK*

(Manuscript received 8 November 2001; in final form 21 May 2002)

ABSTRACT

The surface climatology of Coats Land, Antarctica, is described through observations from automatic weather stations, from Halley station, from upper air soundings and from satellite remote sensing. Coats Land consists of the Brunt Ice Shelf and the adjoining continent to the south. The topography of this region is typical of much of the Antarctic coastal fringes: a modest slope (5% at most) and relative uniformity across the slope. A basic climatology broken into site and season is presented. In winter, and to an extent in the equinoctial seasons, the region clearly divides into two dynamical regimes. Over the ice shelf winds are usually from the east or occasionally from the west, whereas over the continental slopes winds are from the east to south quadrant. Over the ice shelf the surface layer is about 10 K colder, in terms of potential temperature, than on the continent, and is also more stable than on the steeper parts of the slope. Motivated by case studies, three criteria are developed to select a subset of the data that are katabatic in the sense that the flow is believed to be primarily due to a downslope buoyancy forcing. On the continental slope, the criteria pick out a coherent subset of the data that are tightly clustered in wind speed and wind direction. Typical katabatic winds are from 10° to the east of the fall line and 7.5 m s⁻¹ at the steepest part of the slope (5.1 m s⁻¹ higher up). They are rarely more than 15 m s⁻¹ in this region; hence their description as ordinary, in contrast with those extraordinary katabatic regimes that have been the focus of previous studies. The katabatic flow remains close to adiabatic as it moves down the slope, and is relatively dry near the slope foot. We estimate the flow to be primarily katabatic at most 40–50% of the time, although it may appear to be katabatic, from wind speed and wind direction characteristics, some 60–70% of the time. There is no coherent katabatic-flow signature on the ice shelf.

1. Introduction

The observed surface wind pattern over the Antarctic continent is one of a remarkably constant radial outflow from areas of high topography downslope towards the coastline (e.g. Schwerdtfeger, 1984; Parish, 1988). The dominance of this pattern means that the surface flow plays an important role in the tropospheric circulation of the Southern Hemisphere, as well as the climate system in general; for example, through interactions with sea ice and the ocean

through coastal polynyas. The unwavering directional constancy of the surface winds observed at many Antarctic stations (e.g. Schwerdtfeger, 1984; Parish, 1988; Bromwich, 1989b), suggests that topography plays a governing role in determining the local wind field. Indeed for many years it has been suggested that katabatic forcing was dominant in determining the continental surface wind pattern (Ball, 1960; Schwerdtfeger, 1984; Parish, 1988; Parish and Bromwich, 1987; 1991), the premise being that the surface wind pattern is primarily driven by a long-wave radiative cooling of the continental snow surface. This cools the overlying atmospheric surface layer and in the presence of a slope induces a downslope pressure-gradient force, i.e. a katabatic force. However, this

*Corresponding author.
e-mail: i.renfrew@bas.ac.uk

hypothesis does not immediately marry with the many summertime observations, which also show remarkable directional constancy (e.g. Schwerdtfeger, 1984; Parish, 1988; Bromwich, 1989b). In the summertime the radiation balance is not one of constant radiative cooling, indeed it can be positive (the surface gaining energy) over the season (e.g. King et al., 1996). During the summertime the katabatic forcing is often small or non-existent, whilst the wind direction can remain remarkably constant, so what is driving this flow?

Recently a number of studies have started to re-evaluate the premise of a katabatic forcing being the primary driver of Antarctic winds. Parish and Cassano (2001) examined the surface winds in one year of the NCEP/NCAR reanalysis and indirectly calculated the terms of the horizontal momentum equations. They found that the 'pure' katabatic and the 'synoptic-scale' pressure-gradient terms account approximately equally for the surface wind pattern generated by the model. They concluded that the adjustment of the synoptic pressure distribution to the Antarctic topography caused a high degree of directional constancy in the surface wind field of the model. Van den Broeke et al. (2002) and Van den Broeke and Van Lipzig (2002) come to similar conclusions, i.e. a balance between large scale and katabatic forcing appears to govern the surface flow in their model data. They calculate the various terms of the momentum budget explicitly. Parish (2001) presents a series of numerical modelling experiments of an idealised sloped terrain, initialised with different synoptic-scale basic states and model conditions. He found qualitatively similar flow fields over the continent for a surprisingly broad variety of initial conditions. For example, simulations of katabatically driven surface winds were remarkably similar to simulations of non-katabatic winds forced by a meridional pressure gradient or a synoptic-scale low-pressure system. This suggests that, in his model at least, the topography is moulding the surface wind pattern, and the forcing mechanism cannot be deduced from the direction and magnitude of the winds alone.

In terms of observations, a comprehensive investigation of springtime flow over Greenland has recently been completed by Heinemann (1999), where nine case studies were dissected using automatic weather station (AWS) data and aircraft observations. The high density of quality data, such as atmospheric profiles from the aircraft, allowed a full force-balance calculation to be completed. For these nine cases, Heinemann found that the pure katabatic forcing term was largest in each one, although in many the synoptic forcing con-

tributed significantly to the momentum equation, and furthermore the Coriolis force balanced much of the downslope forcing. Without the benefit of a network of high-resolution atmospheric profiles, it is not possible to emulate this type of study, and so for Antarctica a comprehensive observational approach has not yet been possible. During the summer, a few studies have attempted to calculate forcing terms using a limited number of profiles (e.g. Kodama et al., 1989; Liu and Bromwich, 1997; Bintanja, 2000), but it is not wise to generalise these results to the wintertime situation.

Reviewing the above, one is under the impression that there is currently a shift in the perception of what drives Antarctic surface winds. It is within this context that we present a climatology of Coats Land, a region of Antarctica that is typical of much of the coastal fringes of the continent. Indeed the surface winds here could be described as 'ordinary', in contrast to the regions of katabatic convergence that yield extraordinarily strong surface winds (e.g. Bromwich, 1989b; Wendler et al., 1993). The topography of Coats Land is broadly two-dimensional and smooth, rising from around 50 m on the Brunt Ice Shelf to around 1700 m approximately 150 km inland. The slopes are typical of the continent's fringe, about 5% on the steepest point, decreasing with distance inland. The British Antarctic Survey's Halley station is located close to the coast on the Brunt Ice Shelf, and marks the end point of a transect of AWSs running down the fall line of Coats Land. The AWS data, along with upper air and surface-based data from Halley, and some satellite remotely sensed data, form the basis of this study. In section 2 the geography and data sets are described in detail. In section 3 a basic climatology is presented, followed by a brief examination of two case study periods in section 4. Section 5 attempts to address the nature of the surface flow, by 'fingerprinting' primarily katabatic and non-katabatic flow, thus addressing the issues raised earlier in this section. Section 6 concludes the paper.

2. Geographic setting and data coverage

The topography of Coats Land, as extracted from the Antarctic Digital Database Version 3, is shown in Fig. 1 (BAS et al. 1993). The map also shows Halley and four AWS sites: Coats Land AWS sites abbreviated as C1–C4. Table 1 notes some geographical details of the sites. The locations are approximate, as the ice sheet is flowing towards the coast at up to a few hundred metres per year. Halley is on the Brunt Ice

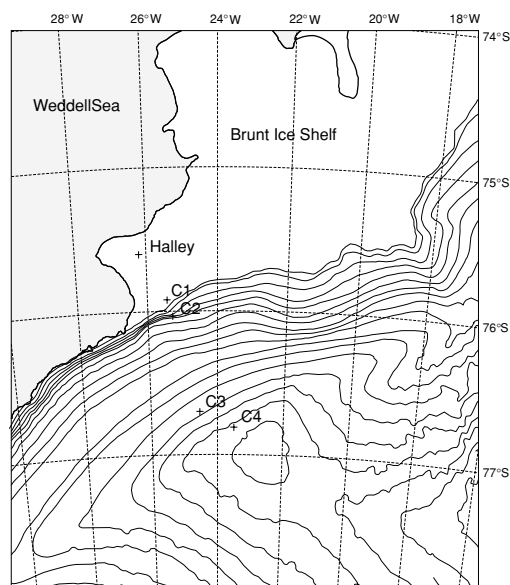


Fig. 1. A topographic map of Coats Land, Antarctica, based on the Antarctica Digital Database Version 3. The contour interval is 100 m. The location of Halley and the four AWS sites are marked (C1–C4).

Shelf, approximately 10 km from the coast. C1 is located 37 km inland from Halley, also on the Ice Shelf, and is just before the 'hinge zone' where the ice sheet leaves the continent and starts floating on the ocean, i.e. at the glacier grounding line. As the name suggests, the hinge zone is a heavily crevassed area, although the C1 site is relatively undisturbed and nominally flat. The remaining sites are all located on the continent itself. C2 is located a further 10 km inland, above the hinge zone, and at approximately the steepest part of the slope. C3 is located a further 86 km inland, with C4 another 32 km beyond, both on relatively gentle slopes. The snow surfaces at all three continental sites are relatively smooth. As illustrated in Fig. 1 the topography of Coats Land is relatively two-dimensional,

and being entirely ice-covered the gradient is smooth. These features suggest that the AWS-based climatology presented here should be representative of the region, and is typical of much of the ice shelf fringed coast of Antarctica.

Halley is a meteorological observing station making 3-hourly synoptic observations and daily radiosonde launches. Here we make use of the operational cloud observations, plus hourly pressure and wind data. The winds are measured at 4 m by a cup-vane anemometer, which is checked daily for rime build up. The wind data tabulated here are corrected to 3 m using a neutral logarithmic wind profile, and assuming a roughness length of 1×10^{-4} m (King and Anderson, 1994). In addition, a number of research instruments have been sited at Halley for use in boundary-layer meteorology experiments. Here we use temperature and humidity measurements at 2 and 4 m, from Vaisala HMP35A sensors housed in R. M. Young force-ventilated radiation shields. King and Anderson (1994) discuss instrumentation at Halley in more detail.

At the Coats Land sites an AWS records hourly station pressure; air temperature and humidity at two heights (nominally 1 and 2.5 m); and winds at one height (nominally 3 m). The temperature and humidity data are from Vaisala HMP35D sensors housed in a modified R. M. Young naturally ventilated shield, where an internal solar-powered fan assists ventilation during periods of strong insolation. The HMP35 range of instruments employed at Halley and the AWS sites use 1/30 DIN platinum resistance thermometers and solid state capacitive humidity sensors. The wind data are from an R. M. Young propeller-vane anemometer. It was found that this design is less susceptible to becoming frozen into position. The AWS pressure and wind data are laboratory calibrated prior to deployment and the pressure sensors are checked annually on site against a Vaisala PA11 digital barometer, which itself is calibrated annually by the UK Met

Table 1. Geographical data for Halley and the Coats Land automatic weather stations (C1–C4)

Station	Latitude	Longitude	Height (m)	Slope (%)	Fall line	Distance from Halley (km)	Distance to downslope station (km)
Halley	−75.60	−26.20	37	0.07	155	0	—
C1	−75.88	−25.49	43	0.7	160	37	37
C2	−75.96	−25.41	400	5.5	165	46	10
C3	−76.70	−24.53	1400	1.0	150	132	86
C4	−76.81	−23.50	1650	0.8	145	155	32

Office calibration laboratory. The temperature data are calibrated in two stages: firstly using a series of precision resistors, which establish a linear correction to the temperatures registered by the AWS, and secondly by making a uniform adjustment of the lower (1 m) temperatures at each AWS, using an offset determined by averaging all the data with very high wind speeds ($>15 \text{ m s}^{-1}$) and assuming the atmosphere is well mixed by mechanical turbulence under such conditions. The second calibration step involves corrections of only $\sim 0.1 \text{ }^\circ\text{C}$, and is carried out to remove discontinuities in the time series and to obtain more reliable surface heat flux estimates. The temperature calibrations are implemented separately for each AWS and each year. The relative humidity data are post-calibrated for each sensor and each year following the method of Anderson (1994). This makes use of the fact that over a snow-covered surface the atmosphere is saturated with respect to (w.r.t.) ice much of the time (e.g. King and Anderson, 1999). The capacitive sensor acts as a nucleation site when the atmosphere is supersaturated, and thus a well defined relative humidity versus temperature upper bound can be obtained by curve-fitting to the data. This method is extremely robust and circumvents the on-site calibration problems inherent in using capacitive humidity devices to give reliable sub-saturated humidity measurements. Most previous AWS-based studies have ignored humidity, due to the calibration problems: here we make full use of our moisture observations.

Table 2 illustrates the months of available data from the Coats Land AWSs between 1996 and 2000. A dash indicates a complete (or near-complete) month of data, a blank indicates no data, while a cross indicates that an AWS was not in place at that time. In total we have 22, 27, 24 and 31 months of data from C1, C2, C3 and C4 respectively. There are a number of periods of missing data due to instrumental failure, a long-standing plague of AWSs in Antarctica (e.g. Bromwich, 1989b; Stearns et al. 1993). For example, there have been a few problems with the loggers short-circuiting, prob-

ably due to static during blowing snow and high wind events, and occasionally there have been battery failures. Despite these problems we are fortunate to have reasonable data coverage for every month at every location: sufficient to carry out a detailed climatological analysis.

3. Surface climatology

A basic summary of the surface climatology of Coats Land is presented in Tables 3 and 4, which show mean and distribution data, respectively. The climatology is broken down into seasons, denoted DJF (summer), MAM (autumn), JJA (winter) and SON (spring). In every season the strongest mean winds are at C2, followed by those at C3, with the weakest mean winds on the ice shelf (at either Halley or C1). The vector-mean wind direction is from the SE at C2, from the ESE at Halley, C3 and C4, and from the E at C1. Recall the fall line is $\sim 150^\circ$ (i.e. from the SSE), so the vector-mean wind directions are to the east of the fall line. In general the wind is more southerly during the winter, and the equinoctial seasons, than during the summer season. The surface wind regime is illustrated in Fig. 2, which shows wind roses for DJF and JJA for all five sites. The JJA (winter) wind roses are qualitatively representative of the MAM and SON seasons (not shown). At Halley there is a bimodal distribution with winds most frequently from the E, ESE or ENE; or from the W or WSW. There are relatively few periods of southerly winds, and northerlies are rare; the strongest winds are always from the E or ENE. The winds at C1, 37 km inland, are similar to Halley, although with a greater number of weak southerlies and less westerlies; again the strongest winds are from the east or ENE. In contrast, at C2, C3 and C4 on the continent, the winds are most frequently from the south-east quadrant, with no winds from the west and rarely from the north. At C2 there are strong winds from throughout the south-east quadrant, but most

Table 2. Months of available data (January–December) from the Coats Land AWS stations (C1–C4)^a

	1996	1997	1998	1999	2000
C1	—	—	×	×	×
C2	—	—	—	—	—
C3	—	—	×	—	—
C4	×	×	—	—	—

^aA cross indicates no AWS was deployed at that time.

Table 3. Mean values for each season of measured and derived variables from Halley and the Coats Land AWS^a

	No. of data	U (m s ⁻¹)	Wind direction	Wind constancy	t_a (°C)	θ (K)	$\Delta\theta/\Delta z$ (K m ⁻¹)	RH _{ice} (%)	q_a (g kg ⁻¹)	p (mb)
DJF										
Halley	10186	5.05	92	0.48	-6.7	267.6	0.09	90	2.10	985.6
C1	2906	5.65	88	0.68	-7.9	266.4	0.18	83	1.71	984.8
C2	5753	6.38	117	0.70	-8.4	269.5	0.07	78	1.64	939.7
C3	5161	5.65	91	0.66	-16.2	271.9	0.07	87	1.06	819.9
C4	6340	4.64	94	0.59	-15.6	274.3	0.11	86	1.12	801.4
MAM										
Halley	10596	5.05	107	0.38	-21.9	252.6	0.32	97	0.66	982.1
C1	4416	4.41	94	0.57	-19.5	255.2	0.22	85	0.70	979.0
C2	7099	7.31	122	0.74	-17.7	260.4	0.22	80	0.77	933.9
C3	4831	6.28	115	0.66	-25.9	262.1	0.21	94	0.48	815.1
C4	6624	5.09	109	0.56	-27.1	263.2	0.40	95	0.44	795.6
JJA										
Halley	10368	5.25	103	0.41	-28.1	246.1	0.41	99	0.39	984.2
C1	4416	5.20	89	0.57	-24.6	249.9	0.38	87	0.45	982.0
C2	2208	9.41	129	0.76	-21.2	257.1	0.31	75	0.51	932.6
C3	4416	6.66	105	0.68	-30.9	256.9	0.21	95	0.30	814.6
C4	5136	5.07	115	0.59	-30.9	259.3	0.54	95	0.30	793.8
SON										
Halley	10438	5.71	95	0.50	-19.5	254.9	0.25	94	0.83	983.0
C1	4340	5.88	90	0.58	-17.0	257.5	0.18	82	0.89	981.7
C2	2184	8.72	121	0.76	-17.3	261.0	0.19	76	0.78	933.0
C3	2373	6.72	107	0.68	-24.4	263.9	0.12	90	0.53	813.7
C4	4360	6.28	100	0.61	-25.5	265.1	0.21	89	0.50	795.2

^aThe first column notes the number of hourly data points available; in general this is the number of points that make up the mean, although note that some data are 'bad', i.e. at C1 the wind data during 1997, and at C4 the pressure prior to 1999. The subsequent columns are wind speed (U), vector-averaged wind direction, wind directional constancy, 2.5 m air temperature (t_a), 2.5 m potential temperature (θ), stability ($\Delta\theta/\Delta z$), relative humidity with respect to ice (RH_{ice}), specific humidity (q_a) and pressure (p).

frequently from the east. The wind roses at C3 and C4 appear similar to C2 except rotated through $\sim 30^\circ$. Strong southerly flow only occurs at C2. Comparing the summer and winter wind roses, there are a few qualitative differences. On the ice shelf, there are more frequently winds from the south during the winter. At C2 there are occasionally winds from the ENE in summer, but rarely in winter. In general there is a greater frequency of stronger winds during the winter. Illustrated as wind roses it is clear that the ice shelf sites are under a qualitatively different surface-flow regime than the continental sites. A fact all the more remarkable when one considers that the C1 and C2 sites are only 10 km apart. This downslope change in flow regime was first hypothesised by King (1993) on the basis of wind data from two ice shelf sites. Examining the complete transect of wind data, we have now shown this hypothesis to be true.

Wind speed distributions are not, in general, close to Gaussian but rather are commonly approximated by a

two-parameter Weibull distribution (e.g. Justus et al., 1978; Pavia and O'Brien, 1986). The two parameters are a scale parameter (α) and a dimensionless shape parameter (β). The scale parameter is linearly related to the distribution mean. The shape parameter determines the skewness of the distribution. The probability density function decreases monotonically when $\beta < 1$, and has a maximum away from zero when $\beta > 1$. It is an exponential distribution when $\beta = 1$, a Rayleigh distribution when $\beta = 2$ and is approximately Gaussian when $\beta = 3.6$ (Pavia and O'Brien, 1986). We have fitted Weibull distributions to the wind speed observations using a simple mean and variance method (Justus et al., 1978), and the results are shown in Table 4. At the ice shelf sites, the shape parameters are 1.0–1.6 indicating an extremely skewed distribution: a high frequency of low wind speeds and a long 'tail' of high wind speeds. These distributions suggest many periods of calm or low wind speeds, frequently punctuated by strong wind events, perhaps due to the

Table 4. Distribution values for each season of measured and derived variables from Halley and the Coats Land AWS^a

	Wind scale parameter (m s ⁻¹)	Wind shape parameter	θ (K)	$\Delta\theta/\Delta z$ (K m ⁻¹)	RH _{ice} (%)	q_a (g kg ⁻¹)	p (mb)
DJF							
Halley	5.63	1.6	5.0	0.25	8	0.76	7.9
C1	6.24	1.5	4.3	0.28	13	0.57	7.8
C2	7.17	1.8	4.4	0.19	14	0.65	6.9
C3	6.36	1.9	5.1	0.23	12	0.46	7.2
C4	5.19	1.7	4.5	0.37	13	0.46	7.4
MAM							
Halley	5.54	1.4	7.7	0.46	8	0.50	8.8
C1	4.66	1.2	6.9	0.43	15	0.51	8.2
C2	8.26	2.0	5.0	0.33	16	0.43	8.4
C3	7.08	1.9	5.8	0.39	11	0.28	8.5
C4	5.62	1.5	5.4	0.61	11	0.24	8.9
JJA							
Halley	5.74	1.4	8.0	0.54	3	0.36	10.2
C1	5.23	1.0	6.9	0.59	14	0.36	10.6
C2	10.62	2.1	4.9	0.46	19	0.29	8.2
C3	7.51	2.0	6.2	0.39	10	0.21	9.9
C4	5.59	1.4	5.4	0.65	13	0.18	8.3
SON							
Halley	6.31	1.5	8.7	0.44	8	0.59	10.5
C1	6.35	1.3	8.3	0.42	15	0.63	10.4
C2	9.84	2.1	6.2	0.40	18	0.44	7.4
C3	7.59	2.1	6.3	0.26	13	0.28	11.0
C4	7.07	1.9	6.6	0.44	16	0.32	10.1

^aThe first and second columns tabulate the scale and shape parameters for Weibull distribution fits to the wind data (see text). All other columns tabulate the standard deviations of the variables. For variable definitions see Table 3.

passage of low pressure systems. Indeed an examination of a number of time series plots shows that these high wind-speed events tend to be seen at all stations simultaneously and are concomitant with a local minimum in pressure. On the continent, the wind speed distributions are more symmetric: at C2 and C3 the shape parameters are around 2, while at C4 they are between 1.4 and 1.9. This translates to a high frequency of low to moderate wind-speed events, with fewer periods of calm. The more symmetric wind-speed distributions on the continent are fundamentally different to those on the ice shelf, again suggesting a different flow regime between the continent and the ice shelf.

Returning to Table 3, during the summer the near-surface air temperature (t_a) generally decreases with elevation (i.e. moving inland). However, during the non-summer months the highest temperatures are at C2 (C1 during SON), rather than Halley. These sites

are located within the ‘thermal belt’, a band of high surface brightness temperatures observed in remote-sensing studies such as Nakagawa and Shimodoori (1994). This thermal structure is a product of strong surface–atmosphere coupling. Over the flat ice shelf, there are many periods of calm or very light winds (Fig. 2): periods of quiescent flow allow a strong surface-layer inversion to develop, driven by long-wave radiational cooling of the surface.¹ Thus the low t_a values of the ice shelf are caused by the close coupling of the surface and near-surface air temperatures. In contrast, on steeply sloped surfaces, for example at C2, there are fewer periods of calm or very light winds (Fig. 2), hence there is generally a greater degree of turbulent mixing and downward turbulent heat

¹The strong inversion is seen as high mean values of $\Delta\theta/\Delta z$ in Table 3: compare the wintertime $\Delta\theta/\Delta z$ at Halley (0.41 K m⁻¹) to that at C2 or C3 (0.31 or 0.21 K m⁻¹).

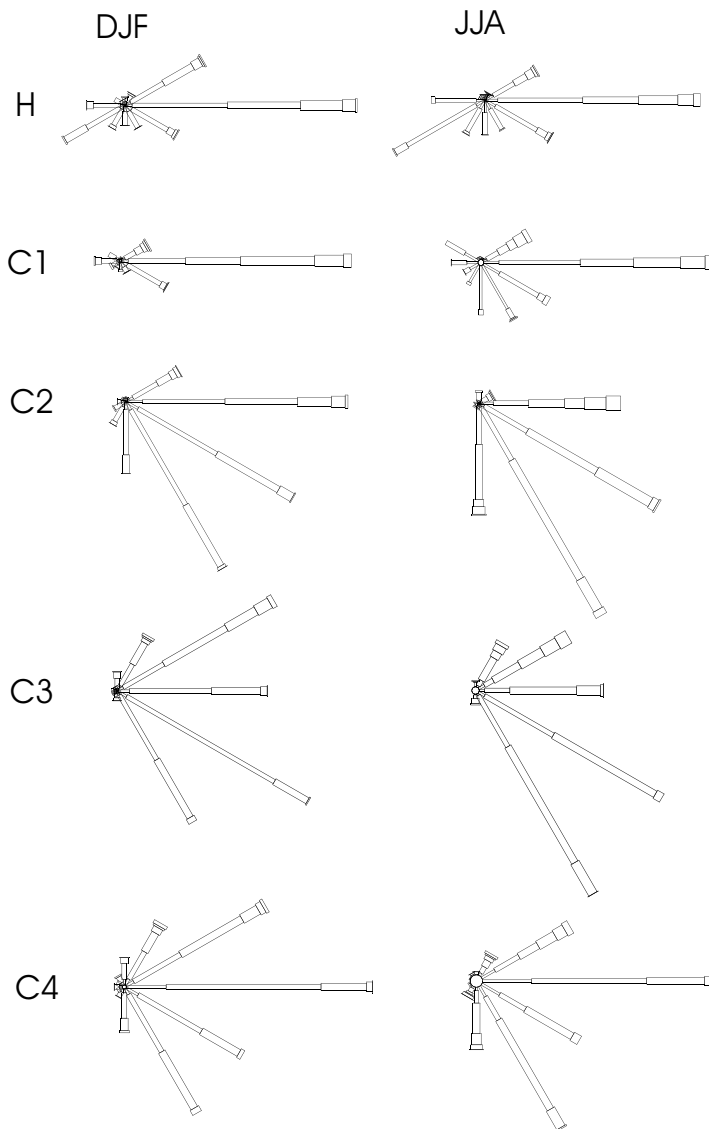


Fig. 2. Wind roses for Halley (H) and C1 to C4 as marked, for summer (DJF) and winter (JJA). The wind directions are divided into 30° bins and the wind speeds into 5 m s^{-1} bins from 0.1 to 30 m s^{-1} . The size of the centre circle is proportional to the number of calm observations.

transfer.² The higher downward surface heat flux leads to higher surface temperatures and thus higher near-

²For example, the mean wintertime surface sensible heat flux (Q_s) at C2 is -43 W m^{-2} compared to -14 W m^{-2} at Halley; so the higher mean wind speed outweighs the lower mean temperature difference.

surface air temperatures. In short, over the ice shelf there is the tendency for a relatively cold and a very stable surface layer, while over the steeper slopes of the continent there is the tendency for a relatively warm and less stable surface layer. The less steeply sloped sites of C3 and C4 are intermediate between these two extremes (Table 3, Fig. 2).

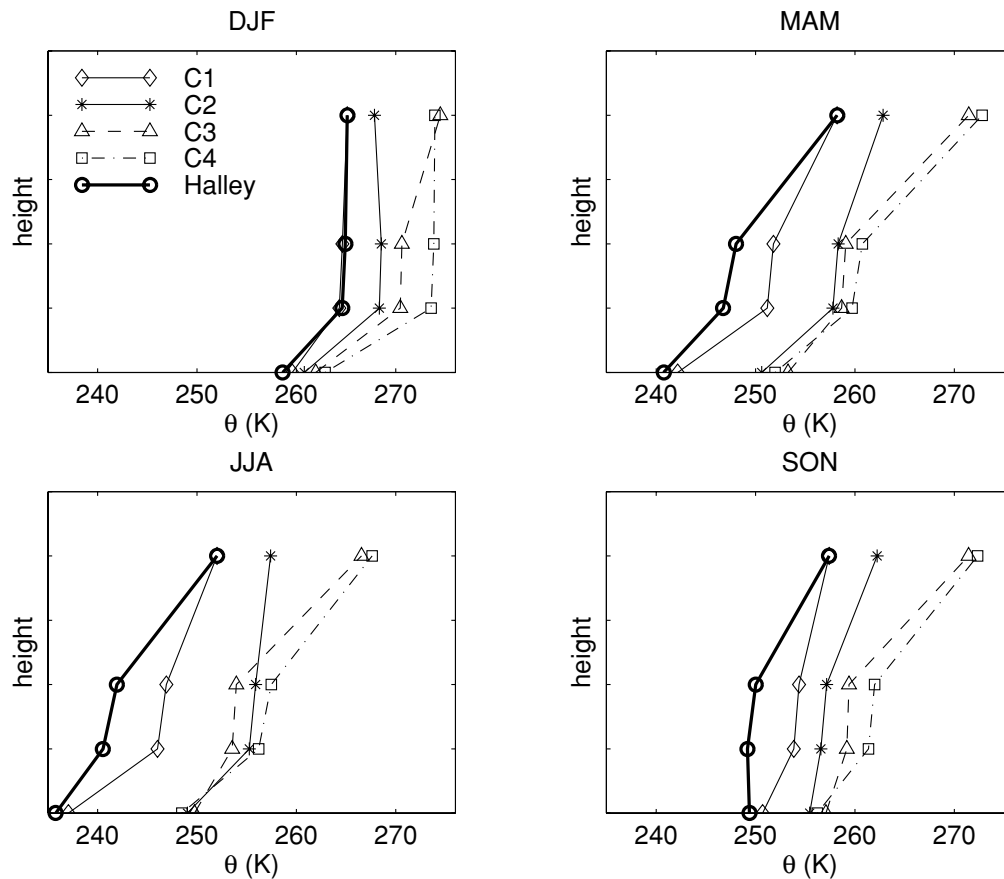


Fig. 3. Illustrations of the mean boundary-layer temperatures for each season during conditionally-sampled clear sky conditions. Note the vertical scale is nominal: the four heights represent the surface, approximately 1 and 2.5 m above the surface, and the free atmosphere (perhaps 50–200 m above the surface). The potential temperatures at the surface are from infrared brightness temperatures (remotely sensed from space); the 1 and 2.5 m potential temperatures are from the lower and upper AWS sensors; and the free-atmosphere potential temperatures are taken from a set of upper air soundings.

In terms of potential temperature (θ), the above equates to a potentially cold surface layer over the ice shelf and a potentially warmer surface layer over the continent, a demarcation that is particularly clear in the winter season (Table 3). This potential temperature picture is consistent with that sketched in King et al., (1998) of an approximately adiabatic surface layer over the continental slope, book-ended by cold and strongly stable surface layers over the ice shelf and over the plateau. In that sketch only *clear-sky* surface temperatures (from remotely sensed infra red satellite imagery) and contemporaneous free-atmosphere temperatures (from upper air soundings at Halley) were used. Hence the climatological data from that study are

conditionally sampled as clear-sky conditions. Here an augmented *clear-sky* boundary-layer thermal structure is illustrated as θ versus height in Fig. 3. The potential temperatures at the surface are from remotely sensed infrared brightness temperatures (from King et al., 1998); the 1 and 2.5 m potential temperatures are from the lower and upper AWS sensors, and the free-atmosphere potential temperatures are taken from a set of upper air soundings (from King et al., 1998). The AWS data are conditionally sampled for when the observed Halley cloud fraction is $\leq 3/8$: this selects $\sim 1/3$ of the available observations. Note: the positions of the heights on the y-axis are *nominal*, and simply represent the relative positions of the surface, the lower

and upper AWS sensors (the surface layer), and the free-atmosphere. The figure illustrates a division of the surface layer into potentially cold over the ice shelf (at Halley and C1) and potentially warm over the continent (at C2, C3 and C4) for clear skies. This is true for all four seasons, but is most marked in MAM and JJA; during SON and DJF incoming solar radiation affects the more northerly ice shelf sites to a greater degree than the continental sites. In addition, the surface layer is approximately adiabatic in the horizontal between C2 and C4 during MAM and JJA. In the non-summer months, the strongest clear-sky surface-layer stabilities are at Halley, C1 and C4. Note that the jump in θ between the surface layer and the free atmosphere is much greater at C3 and C4 than at Halley or C1. At C2 there is little jump in θ between the surface layer and the free atmosphere, perhaps due to a greater degree of turbulent mixing due to the higher mean winds at this site.

In table 3 the moisture content is shown both as relative humidity w.r.t. ice (RH_{ice}) and as specific humidity (q_a). As noted earlier, over an ice surface the atmosphere is close to saturated w.r.t. ice much of the time, so the mean RH_{ice} is high at all the sites. In the winter, it is driest at C2, where $RH_{ice} = 75\%$, compared to Halley where $RH_{ice} = 99\%$, and higher up the slope where $RH_{ice} = 95\%$. If the surface layer is approximately adiabatic, i.e. θ is approximately conserved on the continental slope (Fig. 3), one might expect q_a to also be conserved and for the differences in RH_{ice} to be due to adiabatic warming. However, examining the q_a column in Table 3 shows this is not the case: q_a at C2 is consistently higher than at C3 and C4, which means there is a flux of moisture into the surface layer.

Surface sensible and latent heat fluxes have been calculated using the temperature and humidity measurements at two heights and following a profile bulk-flux methodology. In this case we use a surface roughness length of 1×10^{-4} m, and use the limited-value flux-profile relations of King et al. (1996). Although it is robust, the profile method is extremely sensitive to small changes in temperature or humidity difference, which means unphysically large fluxes can be calculated (e.g. Stearns and Weidner, 1993). To try and eliminate these erroneous fluxes the temperature and humidity difference data are neglected if $t_1 - t_0 > 10^\circ\text{C}$ on the stable side, and $t_1 - t_0 < -0.5^\circ\text{C}$ on the unstable side. The unstable side threshold is smaller, as grossly unstable conditions do not occur at Halley or further inland (King and Anderson, 1994). To give an idea of the uncertainty in the calculated fluxes a sensi-

tivity study was carried out, with the following varied: the threshold for 'bad' data on the unstable side was changed to -0.2 and -1.0°C , the roughness length was changed to 0.5×10^{-4} and 1.2×10^{-4} m (King and Anderson, 1994; King et al., 1996), and the instrument heights were changed by -0.5 and $+1.0$ m (the instrument heights are only known exactly when the site is visited). The accumulated (i.e. worst-case) differences for these changes are used to define a range of uncertainty, as shown in Table 5, for each season and site. The ranges are relatively large in the summer, and all year at C1 (where earlier instrumentation was used). To give a quick impression of the uncertainty, where the magnitude of the mean flux is larger than the range the mean is printed in bold. In other words, the bold estimates are more reliable. To concentrate just on these values: Q_s is always negative, i.e. a flux of heat into the snow surface, with the largest magnitude at C2, the windiest site, followed by C4, C3 and then Halley. The mean latent heat fluxes are an order of magnitude smaller than the sensible heat fluxes and have greater uncertainty. To focus on Q_1 in JJA, there appears to be a change of sign from positive at C3 (e.g. due to sublimation) to negative at C2 and on the ice shelf (e.g. due to freezing).

In short, the climate of Coats Land is clearly divided into two regimes. Over the slopes of the continent the winds are from the east to south quadrant with the strongest winds at the steepest part of the slope, and wind speeds tending to be moderate to strong. Moving down the slope the surface layer is approximately adiabatic, but becomes more moist (although drier in terms of RH_{ice}). On the adjoining ice shelf, only a few kilometres north, the surface climate is startlingly different: there is a bimodal wind distribution with winds from either the eastern or western sectors, and with wind speeds much more skewed; i.e. periods of calm to low winds interrupted by moderate to strong wind events. The surface layer is much colder (potentially) than over the slopes.

4. Two case studies

Time series from the AWSs and Halley from May 1999 are plotted in Fig. 4. The panels show wind speed, wind direction, perturbation pressure, total cloud amount (visually observed at Halley), θ , $\Delta\theta/\Delta z$, RH_{ice} and q_a . The perturbation pressure (p') is the deviation from a mean pressure for that month at that site. Thus large differences in p' between

Table 5. Surface sensible (Q_s) and latent (Q_l) heat fluxes for each season and each station, calculated using the profile method described in the text^a

	Mean Q_s (W m ⁻²)	Range Q_s (W m ⁻²)	Std. dev. Q_s (W m ⁻²)	Mean Q_l (W m ⁻²)	Range Q_l (W m ⁻²)	Std. dev. Q_l (W m ⁻²)
DJF						
Halley	-1.4	[-4.0 4.4]	28.4	2.5	[0.9 5.9]	22.4
C1	-18.9	[-25.0 -6.4]	46.2	-4.7	[-7.1 1.0]	27.1
C2	-2.3	[-13.4 25.2]	39.0	25.3	[6.9 63.8]	78.0
C3	-2.7	[-7.5 9.8]	25.9	-1.4	[-2.1 -0.9]	11.7
C4	2.7	[-6.2 20.3]	24.0	2.3	[-0.1 6.8]	8.0
MAM						
Halley	-11.1	[-12.7 -7.1]	21.4	-1.5	[-1.5 -1.3]	5.7
C1	-7.1	[-13.1 3.4]	34.5	0.6	[-0.4 2.1]	7.9
C2	-25.2	[-28.1 -18.6]	31.7	-6.6	[-9.3 -4.4]	32.4
C3	-17.5	[-19.3 -12.9]	26.9	-0.5	[-0.6 0.1]	8.6
C4	-15.4	[-17.5 -10.3]	27.1	-0.4	[-0.7 0.3]	4.0
JJA						
Halley	-13.9	[-16.0 -9.1]	23.8	-1.2	[-1.2 -1.0]	5.8
C1	4.2	[-13.3 27.2]	46.6	2.3	[-0.4 5.3]	8.3
C2	-43.1	[-51.2 -31.2]	39.3	-1.6	[-2.5 -1.1]	24.7
C3	-18.1	[-20.2 -13.4]	24.8	0.7	[0.4 1.1]	4.1
C4	-23.3	[-21.3 -17.6]	31.6	-0.1	[-0.2 0.2]	5.5
SON						
Halley	-8.5	[-11.0 -2.9]	25.3	-1.0	[-1.1 -0.6]	7.5
C1	-2.7	[-17.4 19.8]	48.0	4.3	[1.1 8.8]	13.1
C2	-17.5	[-21.5 -6.5]	43.9	9.0	[3.6 19.2]	29.8
C3	-9.6	[-14.4 0.4]	31.5	-	-	-
C4	-7.7	[-13.0 4.3]	31.3	1.7	[0.5 3.7]	11.9

^a'Best estimate' time series of fluxes are calculated and the seasonal mean and standard deviations are for those series. A range of uncertainty for the mean value is found by varying: the temperature difference cutoff for 'bad' data, the roughness length, and the difference in height of the sensors from their assumed height. The uncertainty from each of these parameters is accumulated to obtain the uncertainty ranges shown. Mean fluxes which have a magnitude larger than this range of uncertainty are shown in **bold**.

the sites indicate that the pressure distribution is anomalous from the mean pressure distribution. Perturbations from a monthly mean are used to nullify the seasonal shifts of mass observed over the Antarctic, a by product of the polar location and elevation of the continent (Parish and Bromwich, 1998). It was found that, interpreted carefully, using p' was a useful indicator of the mesoscale pressure gradient, better than calculating a mean sea-level pressure where the problems of reducing to sea level without a temperature profile are well known (e.g. King and Turner, 1997). However, one should bear in mind that p' does not tell us anything about the 'background' pressure distribution that will exist due to the differential heating between the continent and the surrounding ocean for example.

In the first few days of May 1999 (Fig. 4) there is a period of high wind speeds affecting all the sta-

tions. The winds are from the east and reach over 15 m s⁻¹. At the same time, p' shows a well defined local minimum and a spreading of p' between the stations: this suggests the presence of a low-pressure system to the north of Halley, causing low p' -values and an anomalous meridional pressure gradient. Examination of infrared satellite imagery shows the spiralling cloud bands indicative of a synoptic-scale low-pressure system located in the Weddell Sea (not shown), and indeed the cloud cover observed at Halley is high. It seems this period of high winds is due to this synoptic-scale low-pressure system. Associated with the passage of this low are relatively high potential temperatures and low stabilities at all the stations. The gradient in p' is qualitatively in balance with the baroclinicity evident in θ (C2-C4) over 3-6 May 1999. The initially dry (unsaturated w.r.t. ice) air at C2-C4 becomes saturated on the 4 May 1999, presumably due to turbulent

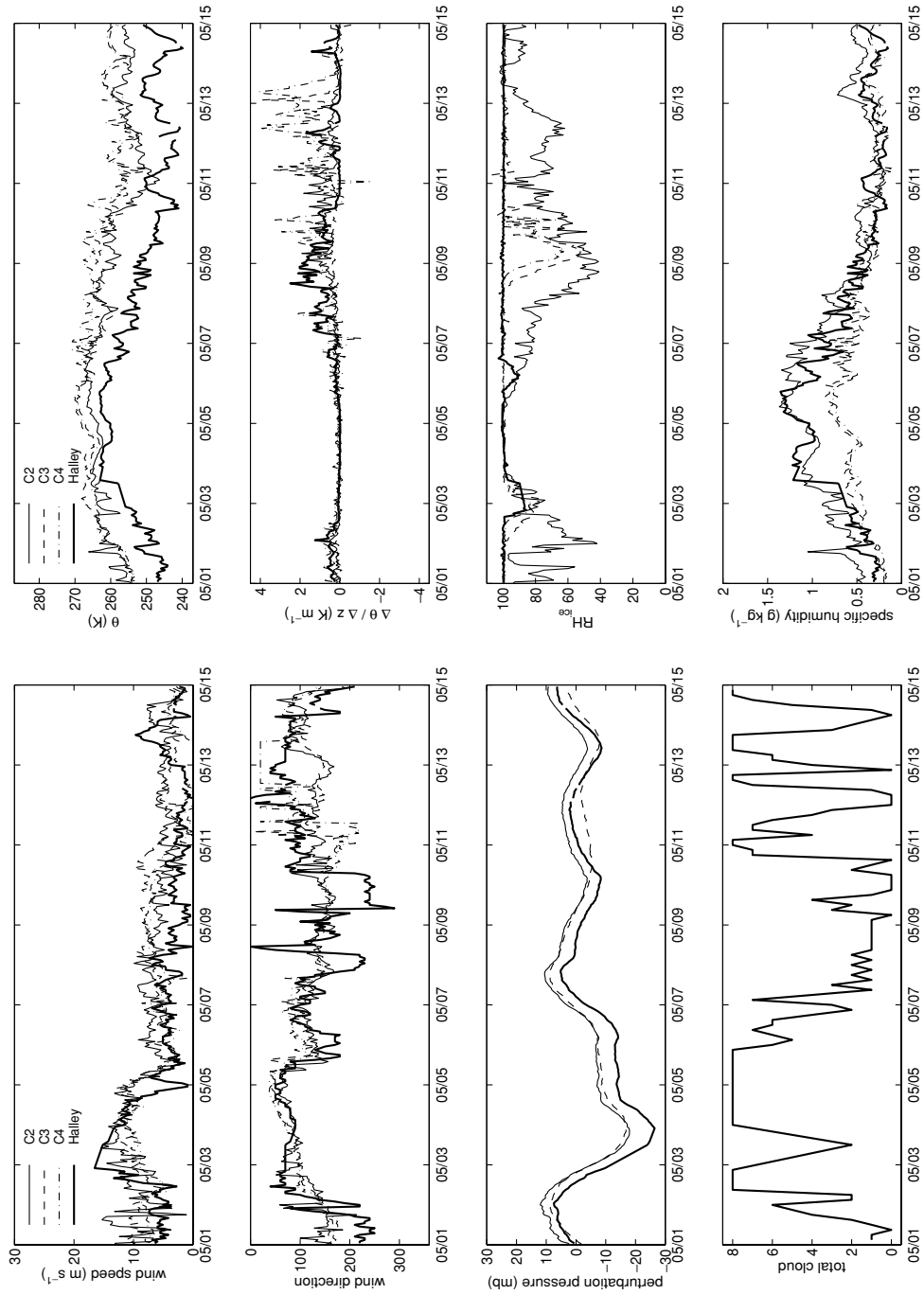


Fig. 4. Time series from 1–15 May 1999 of wind speed, wind direction, perturbation pressure, total cloud amount, potential temperature (θ), surface-layer stability ($\Delta\theta/\Delta z$), relative humidity w.r.t. ice (RH_{ice}) and specific humidity. The ticks mark 00 UTC on each date. The time series are from the Halley and AWS data sets as marked. The perturbation pressure is the perturbation away from the station mean for that month. The temperature and humidity data are from the upper sensors.

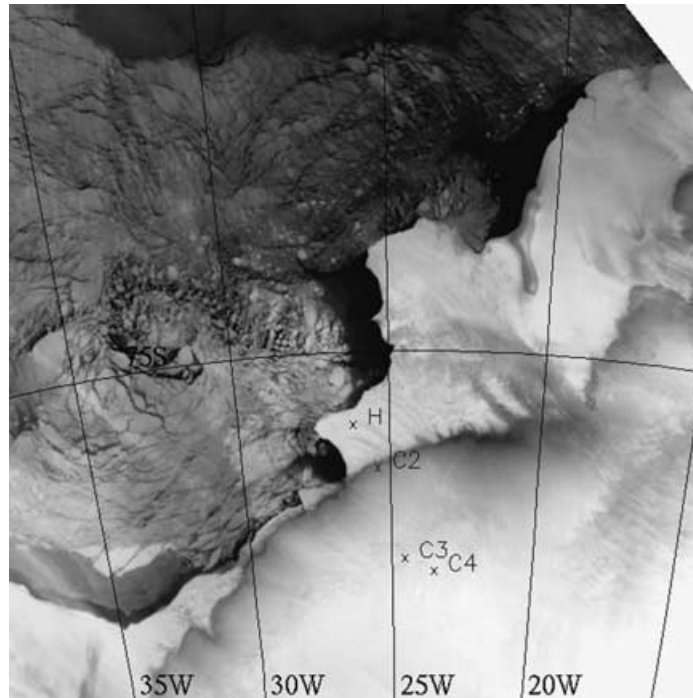


Fig. 5. Infrared AVHRR (Channel 4) satellite image of Coats Land, the Brunt Ice Shelf and part of the sea-ice-covered southern Weddell Sea at 1915 UTC 7 May 1999. The image is produced with warmer brightness temperatures dark. The locations of Halley, C2, C3 and C4 are marked. Features discussed in the text include the 'thermal belt' along the foot of the slope, and the warm signatures of katabatic flows to the east of C2.

mixing of saturated air from the surface and the free atmosphere into the surface layer.

The passage of a synoptic-scale baroclinic low-pressure system between 2 and 6 May 1999 gives way to a period of moderate winds and small p' differences. On 6 May 1999 the winds veer to the SE at all stations and remain around $7\text{--}6\text{ m s}^{-1}$ at C2, and $5\text{--}7\text{ m s}^{-1}$ at C3 and C4 over the next few days. The winds at Halley decrease more markedly to near zero on 9 May 1999. The cloud cover fades to basically clear skies between 7 and 10 May 1999, leading to a cooling (in θ) at all the stations.

A sequence of infrared satellite imagery shows clear skies over the whole of Coats Land between 7 and 10 May 1999. Figure 5 shows one such image from 1915 UTC 7 May 1999. The image has been processed so that lighter colours are colder brightness temperatures, hence colder surface temperatures during clear skies. There are a number of common features in all the infrared images. The Brunt Ice Shelf is clearly visible as a relatively cold surface, with warmer sea ice and polynyas to the north and west. The surface tempera-

tures decrease with height on the continent up to their coldest at the summit. Along the foot of the continental slope is a warm band, the 'thermal-belt' as discussed by Nakagawa and Shimodori (1994), and King et al. (1998). The AWS C2 lies within the thermal belt, in the warmest part of Coats Land, as seen in the climatology (section 3). In addition, this image shows some interesting features: to the east of C2 dark trails emanate from the foot of the slope onto the ice shelf to around 10 km. We suggest these are the thermal signature of moderate katabatic flows, where the enhanced turbulent mixing in katabatics warms the snow surface, relative to the quiescent (strongly stratified) flow on either side, and thus causes a warm signature (e.g. Bromwich 1989a). There are more extensive warm signatures, around 20°W , at the mouth of a valley (Fig. 1) where katabatic flow convergence would be expected. In many of the clear sky images examined there are faint warm bands on the Brunt Ice Shelf, curving from near C2 to near Halley. The persistent nature of these warm bands and an examination of Radarsat images of the region (not shown) suggests that these are due

to glaciological features on the ice shelf. Brightness temperatures can be extracted from these images, as illustrated in Fig. 3, and these are consistent with the surface layer (potential) temperatures of Fig. 4.

Figure 4 illustrates that over the ice shelf there is a very cold and dense surface layer: typically θ is some 10 K colder than on the continent. Firstly at Halley and C4, and then at C2 and C3, there are large positive spikes in surface-layer stability, indicating a strong temperature inversion. We can surmise that this period (from 7–12 May 1999) is one of katabatic forcing leading to moderate downslope winds on the continent. At Halley there is possibly some signature of the katabatic flow at first, with SE winds over 7 May 1999, but by 9 May 1999 the winds have dropped to near zero and are flipping from easterly to westerly. Associated with the katabatic flow are periods of approximately constant potential temperatures and q_a values at the continental sites. These periods appear only to last a few hours before a horizontal θ gradient is again established.³ As the katabatic period takes over, the surface layer over the continent becomes unsaturated w.r.t. ice, firstly at C2 and then C3 and C4. In contrast, over the ice shelf the atmosphere remains saturated w.r.t. ice. By 12 May 1999 the winds have dropped at C4, the highest station, but remain moderate at C2 and C3 until the end of the period, despite the intermittent cloud cover. In summary, this 2 wk period in May shows a transition from a synoptically forced surface flow to a katabatically forced surface flow, which after a day or so transition time affects only the continental sites.

A second time series from June 1998 is shown in Fig. 6. Note that during this period C3 was not in place and there was no pressure sensor at C4. There is a major wind speed event affecting all the stations from 6–8 June 1998; peak wind speeds are over 25 m s^{-1} at C2. Winds are from the east, and there is a meridional p' gradient between C2 and Halley, consistent with a synoptic-scale low-pressure system to the north of Halley. Again examination of infrared satellite imagery shows the characteristic cloud bands associated with a large-scale low-pressure system located in the Weddell Sea (not shown). This is consistent with the observations of large total cloud amounts and the consistent gradient in θ between C2 and C4 during this

period. Associated with the high winds are relatively warm temperatures, and a saturated and well mixed surface layer.

The high winds start to tail off during 8 and 9 June 1998, falling to $8\text{--}12 \text{ m s}^{-1}$ at C2 and $0\text{--}5 \text{ m s}^{-1}$ at C4 and Halley. By halfway through 9 June 1998 there is no p' gradient, the sky is clear, and the surface layer is relatively stable at all the sites; thus the steady SSE flow at C2 appears katabatically forced. A sequence of infrared satellite imagery from 9–11 June 1998 shows clear skies over the whole region (not shown). Associated with this katabatic flow at C2 are RH_{ice} values of around 70–80%. There are periods of much higher stability at C4, but the winds are weaker and more intermittent; the katabatic forcing is less due to the lower slope at C4. At Halley, the surface layer is stable and much colder. In this case the flow at Halley does not fall to around zero, but rather is $\sim 3 \text{ m s}^{-1}$ from the south, veering to a steady $\sim 5 \text{ m s}^{-1}$ from the west sustained through 10 and 11 June 1998. So interestingly, the surface flow at C2 is from the SSE at $\sim 8 \text{ m s}^{-1}$ and is katabatic, but only 50 km away at Halley the flow is from the west at $\sim 5 \text{ m s}^{-1}$, a dramatic change.

The adjustment of a downslope flow on reaching a flat surface is to one of inertial balance, thus in the Southern Hemisphere, for example, a turning of southerly flow towards an easterly. For the June case above, one would expect a steady 10 m s^{-1} flow from 160° at C2 to back to 100° at Halley, whereas we observe the flow to be from around 250° at Halley. The same is true in the May 1999 case: the wind directions at Halley are not those expected of a simple turning of the flow. It would appear that over Coats Land the situation is more complicated than a simple adjustment to inertial balance.

To investigate this case further, Fig. 7 shows θ and U profiles from the midday radiosonde soundings at Halley on 7, 8 and 10 June 1998. On 7 June 1998 the 20 m s^{-1} surface winds (Fig. 6) are accompanied by winds of over 30 m s^{-1} through the troposphere. The atmosphere is stable but there is no strong surface-layer temperature inversion. By the next day there is a $\sim 15^\circ\text{C}$ temperature inversion, and the whole troposphere has cooled some 5°C . There is a pronounced 20 m s^{-1} low-level jet in wind speed, but winds of only 10 m s^{-1} aloft. By 10 June 1998 the winds have dropped further and the temperature inversion is still strong. The troposphere has warmed slightly and the winds are from the west veering to the north over 1000 m (not shown). The fundamental change in

³Comparing temperatures between stations where the exact height of the instruments is not precisely known is bound to include some bias due to instrumental height differences, especially given the large lapse rates observed here.

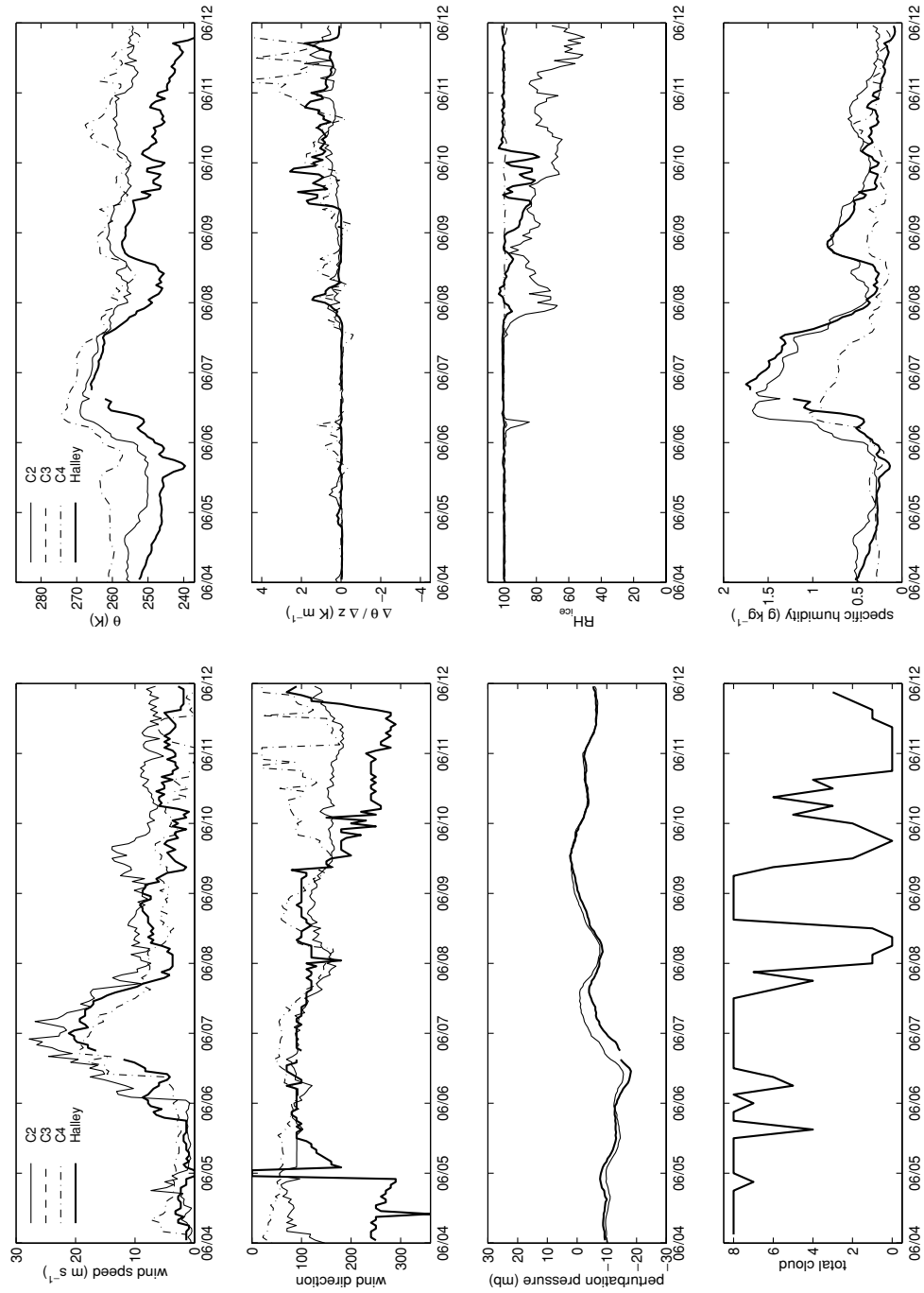


Fig. 6. Time series from 4–12 June 1998 of wind speed, wind direction, perturbation pressure, total cloud amount, potential temperature (θ), surface-layer stability ($\Delta\theta/\Delta z$), relative humidity w.r.t. ice (RH_{ice}) and specific humidity; as for Fig. 4.

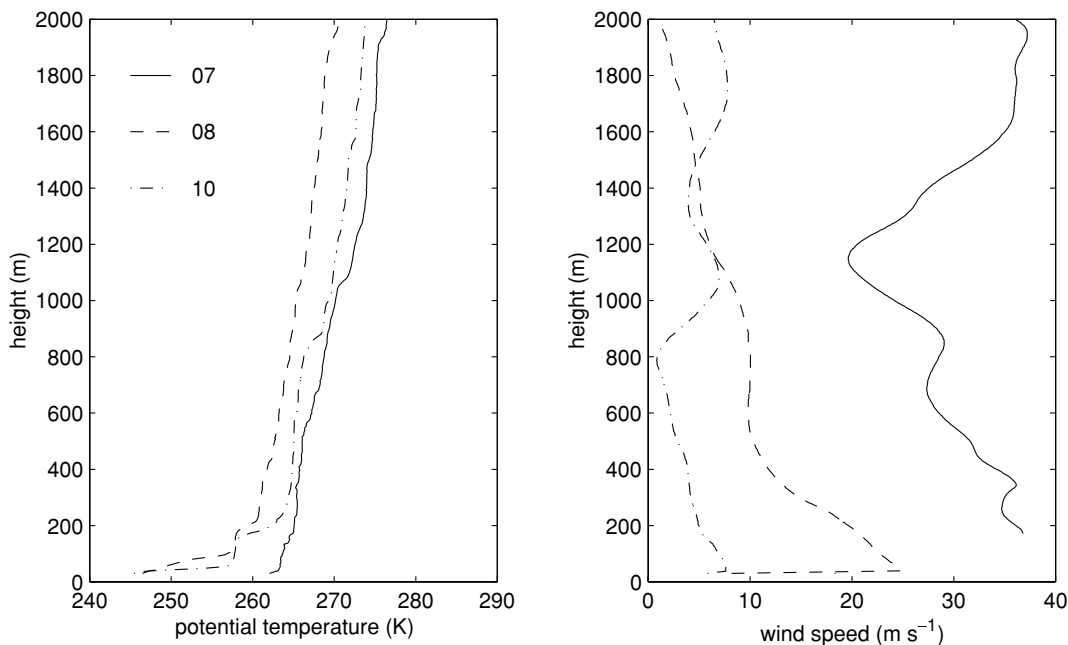


Fig. 7. Profiles of potential temperature and wind speed from upper air soundings taken at Halley on the 7, 8 and 10 June 1998.

regime after the strong wind event is the cooling of the ice shelf and the establishment of a very cold surface layer overlying it. The potential temperature profile, in this case, means that below about 150 m in height the atmosphere is colder, and therefore more dense, than the near-surface air at C2 and C3 (Figs. 6 and 7). Hence in this case we conjecture that the katabatic flow that is influencing the continent is not observed at Halley due to the cold air damming of the ice shelf surface layer. The katabatic flow must somehow be dispersed between C2 and Halley. We suggest that once the pool of cold dense air is established the katabatic flows over and mixes with this surface layer in the vicinity of the slope foot; such a mixing would force the katabatic flow from supercritical to subcritical (shooting to tranquil flow) in terms of a hydrodynamical framework (e.g. Ball, 1960; Gallego and Schayes, 1992; Gallego and Pettre, 1998; Heinemann, 1999). In general, a hydraulic jump is not required as the katabatic can simply flow over the top of the dense ice-shelf air, but in this case there is no evidence of such a flow. A further investigation of such phenomena is being pursued through more detailed case studies and with the aid of numerical modelling studies.

5. Fingerprinting katabatic flow

It is clear from the surface climatology and the cases studies discussed in the previous two sections that Coats Land does not experience solely katabatic flows, but rather a mix of katabatics and winds primarily forced by other types of weather system. Here we refer to katabatics, or katabatic flows, as those believed to have been dominated by a downslope buoyancy forcing. It is tacitly accepted that there may be an element of katabatic forcing in flows which are primarily forced by larger-scale weather systems. In this section we firstly attempt to characterise the katabatically forced flows of Coats Land and secondly examine how often they occur.

To start we define three simple criteria to obtain a subset of the AWS observations that are, we believe, primarily katabatic. Given the limitations of a surface-based data set it is not possible to establish this beyond doubt, as a momentum budget calculation is not possible; however, our results provide us with confidence in the methodology. The criteria are: (1) the data are from June, July or August, so that the surface radiation balance is a net cooling to space; (2) the meso-scale pressure gradient is small, so that

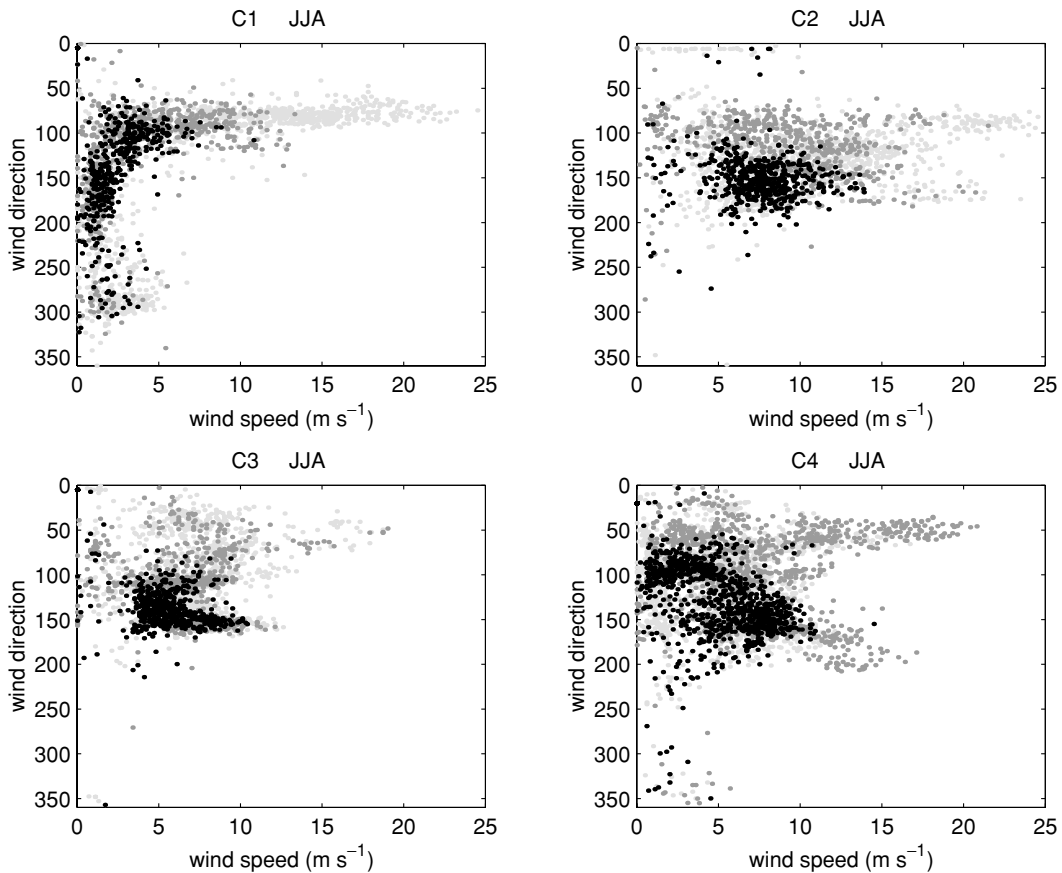


Fig. 8. An illustration of the 'primarily katabatic' selection criteria via scatter plots of wind speed versus wind direction. The light grey dots show all matching JJA data. Over-plotted as dark grey dots are the subset of data where $\nabla p'$ is between the 1/4 and 3/4 quartile of the $\nabla p'$ distribution, where $\nabla p'$ is between the station and Halley. Then over-plotted in black are the subset of data where $\Delta\theta/\Delta z > 2/4$ quartile of the $\Delta\theta/\Delta z$ distribution, where $\Delta\theta/\Delta z$ is at the station. The black dots shows the distribution of katabatic flows in wind speed and wind direction space.

the influence from larger-scale weather systems is reduced; and (3) the surface layer is stable, and as such can exert a katabatic forcing. The selection process is illustrated in Fig. 8, which shows wind speed versus wind direction scatter plots for C1–C4. The light grey dots are all the JJA data where observations are available from both the station and Halley (criterion 1). Over-plotted in dark grey are times when $\nabla p'$ (between the station and Halley) is between the 1/4 and 3/4 quartiles of the $\nabla p'$ distribution (criterion 2). Then over-plotted in black are times when $\Delta\theta/\Delta z$ is greater than the 2/4 quartile of the $\Delta\theta/\Delta z$ distribution (criterion 3). Hence the black dots in Fig. 8 represent our defined 'primarily katabatic' data. It is apparent that this procedure selects a coherent subset of the data at

C2, C3 and to a lesser extent at C4, at least in terms of wind speed and wind direction characteristics. At C2 and C3, the black dots identify data of moderate wind speed and with a preferred wind direction. At C4 the black dots appear to have two clusters, one of low wind speed and a direction around 100° , one of moderate wind speed and a direction around 150° . Neither very high nor very low wind speed data are selected at any of the continental sites; indeed Fig. 8 suggests almost all the high wind speed events are forced by large-scale pressure gradients. At C1 (as well as Halley, not shown) the black dots are spread throughout wind speed–wind direction space; i.e. these criteria do not appear to pick out a coherent flow on the ice shelf.

Table 6. Summary of winter time ‘primarily katabatic’ flow characteristics at the three sites on Coats Land, showing the mean (and standard deviation) of the basic atmospheric variables^a

Station	No. of data	U (m s ⁻¹)	Wind direction	Wind constancy	Wind shape parameter	θ (K)	RH _{ice} (%)	q_a (g kg ⁻¹)	Q_s (W m ⁻²)	Q_l (W m ⁻²)
C2	543	7.5 (2.3)	153 (27)	0.89	3.6	257.1 (3.0)	67 (17)	0.42 (0.13)	-73 (30)	-1.1 (20)
C3	949	5.1 (2.4)	139 (46)	0.85	3.5	254.0 (4.3)	94 (10)	0.20 (0.09)	-31 (19)	-0.5 (1.5)
C4	553	3.8 (2.5)	132 (43)	0.73	1.6	257.2 (4.1)	96 (11)	0.24 (0.10)	-32 (35)	-0.5 (5.4)

^aThe katabatic flow data are chosen using the following criteria: (1) data are from June, July or August; (2) the meso-scale pressure gradient is small (in this case $\nabla p'$ is between the 1/4 and 3/4 quartiles, using p' from the station and from Halley); and (3) the surface layer is stable (in this case $\Delta\theta/\Delta z$ is greater than the 2/4 quartile at the station).

Following the criteria illustrated above, Table 6 summarises the ‘primarily katabatic’ flow characteristics for the Coats Land stations. At C2 and C3 the wind constancy is over 0.85 and the wind shape parameter is approximately 3.6, i.e. the wind distribution is approximately Gaussian (c.f. section 3). This indicates that these data are part of a coherent flow with, in all likelihood, a common forcing mechanism; in this case they represent katabatically forced flow. A Gaussian wind distribution signifies that the flow is well represented by its mean and standard deviation. Hence we can say the mean katabatic wind is 7.5 m s⁻¹ and from 153° at C2, and is 5.1 m s⁻¹ and from 139° at C3. These wind directions are approximately 10° to the east of the fall line (Table 1). The bimodal wind speed distribution at C4 means the wind constancy is lower (0.73) and the wind shape parameter is more skewed (1.6). At C4 the katabatic criteria appear to pick out two regimes: a more quiescent flow from the east and a more dynamic flow from the SSE (Fig. 8). The mean wind direction is still around 10° to the east of the fall line. The potential temperatures during katabatic flow are similar to climatology (Table 3), although the standard deviations are somewhat smaller, perhaps due to

the removal of periods of calm conditions when strong temperature inversions can develop. Another characteristic of the katabatic flow is its relative dryness lower on the continental slope: the mean RH_{ice} at C2 is 67%, compared to 75% for all JJA data. Given the selection criteria, it is not surprising that the surface turbulent heat fluxes are higher during katabatic periods than in the climatology.

So far we have characterised katabatic flow on Coats Land by applying our criteria locally at the station. One could ask another question: what does the atmosphere look like when the flow is katabatic at (for example) C2? We choose C2 as this site has the strongest and most coherent katabatics (Table 6). To this end, Table 7 and Fig. 9 summarise data from Halley, C2 and C4 when there are katabatic conditions at C2. The ‘all conditions’ row at each station tabulates means of all matching times within JJA (see also Fig. 9a). The ‘katabatic conditions’ row at each station tabulates means of the subset of data where the above katabatic criteria are applied at the C2 site, i.e. small $|\nabla p'|$ and large stability (see also Fig. 9b). Unfortunately there are no JJA matching times for C3 and C2.

Table 7. A comparison of the mean characteristics of subsets of data for Halley, C2 and C4^a

Station	conditions	U (m s ⁻¹)	Wind dir.	Wind constancy	Wind shape param.	θ (K)	RH _{ice} (%)	q_a (g kg ⁻¹)	Q_s (W m ⁻²)	Q_l (W m ⁻²)	$ \nabla\theta \times 10^{-6}$ (K m ⁻¹)	cloud amt.
Halley	All	5.4	114	0.51	1.5	247.7	99	0.41	-15	-1.8	-	4.1
	Katabatic	3.3	188	0.37	2.0	246.6	98	0.32	-21	-1.5	-	2.6
C2	All	9.3	129	0.76	2.2	257.1	76	0.51	-43	-1.4	3.4	-
	Katabatic	7.5	153	0.89	3.6	257.1	67	0.42	-73	-1.1	2.6	-
C4	All	4.9	112	0.49	1.5	260.7	96	0.32	-16	-0.2	3.4	-
	Katabatic	3.4	144	0.65	1.4	260.0	96	0.28	-20	-0.1	2.6	-

^aThe ‘all conditions’ rows are for all matching times during the winter (JJA); the ‘katabatic conditions’ rows are all matching times where the katabatic criteria discussed with respect to Table 6 (i.e. small $|\nabla p'|$ and large stability) are applied at the C2 site.

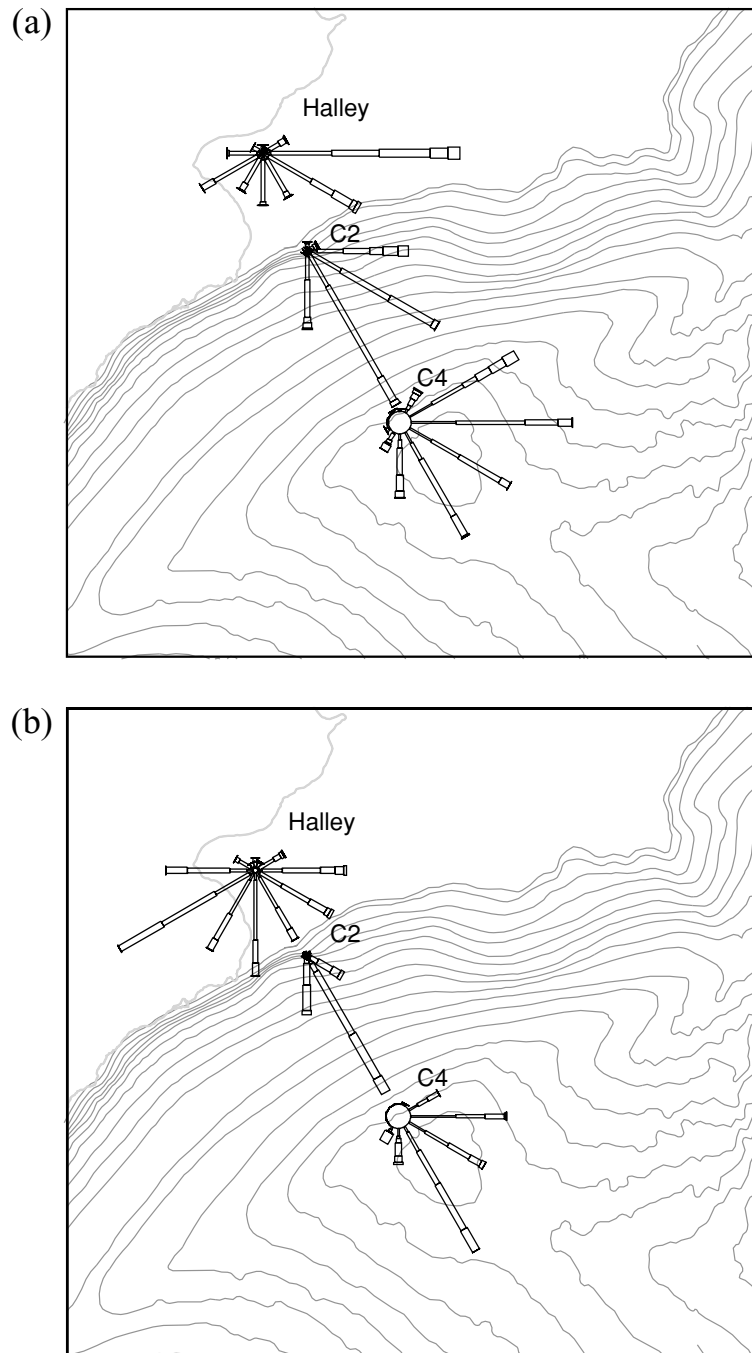


Fig. 9. Wind roses for Halley, C2 and C4: (a) for all matching winter time observations, and (b) during katabatic conditions at C2 (cf. Table 7). Plotted as a background is the 100 m topography from Fig. 1.

At Halley, excluding the large $|\nabla p'|$ data gives a lower mean wind speed and a wind shape parameter of 2.0, i.e. a less skewed distribution. Examining Fig. 9 we see the high wind speed observations from the E and ENE have been deselected. However, the low wind constancy (0.37) and the large spread in the wind rose show that the flow is not 'coherent' in any sense. The surface layer during katabatic conditions is 1 °C colder and there is a smaller total cloud amount. In other words, katabatic conditions on the continent tend to occur when the skies are clearer than average, which allows greater radiative cooling. However, in general, there is no distinctive surface signature at Halley when there is katabatic flow on the continent. At C2, as discussed above with relevance to Table 6, selecting katabatic conditions results in a tightly constrained wind rose. At C4, during katabatic conditions at C2, the flow appears to fall into three clusters: periods of calm, periods of low wind speeds from the E, and periods of moderate winds from the ESE to S (Fig. 9b). The latter two clusters are also seen in Fig. 8, when the katabatic criteria are applied at C4. The first cluster shows that strong katabatic winds may be blowing at C2 while it is flat calm at C4. Comparing directly the katabatic and all data conditions at C4, there is an increase in wind constancy but the wind shape parameter remains similar. Most of the winds from the NE are deselected, including all the high wind speeds. On average the katabatic conditions are marginally colder and drier at C4.

Table 7 also compares the mean horizontal θ gradient (between C2 and C4): this reduces by around 20% during katabatic conditions. On the continent the surface layer is closer to adiabatic in the horizontal during katabatic conditions, as has been seen in a number of numerical modelling studies (e.g. Parish and Waight, 1987).

Making the assumption of a uniform two-dimensional slope (Fig. 1) one can use the mean katabatic conditions data in Table 7 to carry out a heat and moisture budget analysis for a hypothetical air parcel belonging to an *average* katabatic flow. Such budget analyses have been used in the analysis of aircraft data where Lagrangian flight patterns have been performed (e.g. for more details see Bretherton and Pincus, 1995; or Renfrew and Moore, 1999). In using the mean data we have to assume steady-state conditions. The assumption of a uniform slope allows us to assume the air parcel 'passes over' C4 and then C2. From Table 7, the mean differences between C4 and C2 are: $\delta\theta = -2.9$ K, $\delta q_a = 0.14$ g kg⁻¹ and $\delta t = 19705$ s

(5.5 h). The time difference assumes the air parcel travels between C4 and C2 at the average of the mean (downslope) station wind speeds (7.5 and 3.4 m s⁻¹). Within an air parcel one would expect conservation of θ and q_a , and so the differences must be due to sources and sinks of energy and moisture. From the limited observations that exist we know that katabatic flows are typically around 100 m in depth (e.g. Heineemann, 1999). If we take 100 m as the height of our air parcel, the θ and q_a differences equate to sensible and latent heat fluxes of -15 and $+2$ W m⁻², respectively (here a positive sign indicates a flux into the air parcel). Table 7 notes the average (C2 and C4) surface sensible and latent heat fluxes, calculated from the profile method, are -46.5 and -0.6 W m⁻² respectively; which means there are unaccounted for heat and moisture fluxes of -31.5 and 2.6 W m⁻², respectively. We would suggest that the most likely source of this extra heat and moisture is from the turbulent entrainment of warm and moist air into the air parcel from above. Other sources may include mean vertical inflow and radiative flux convergence, which we would suggest are small; as well as microphysical processes, for example sublimation of airborne snow. Sublimation of blowing snow would cool and moisten an air parcel, so we would suggest the above differences represent a minimum bound in $\delta\theta$ and a maximum bound in δq_a . If we assume all the other sources and sinks are negligible, this would suggest downward turbulent entrainment sensible and latent heat fluxes of (at least) 30 W m⁻² and (at most) 3 W m⁻², respectively.

In the Introduction to this paper we noted a current topic of debate was how much apparent katabatic flow is truly katabatically forced, and how much just 'looks' katabatic, in that it has a downslope wind direction. Here we contribute to this debate using the data summarised in Table 6 and Fig. 8. These data suggest primarily katabatic winds at C2 and C3 are strongly unidirectional and have a Gaussian distribution in wind speed. Hence we can define 'katabatic-looking' winds as coming from within ± 2 standard deviations of the mean wind directions, and with a wind speed within say ± 2 (or ± 3) standard deviations of the mean (Table 6). At C2 this definition accounts for 60% (or 72%) of the observations; while at C3 it accounts for 66% (or 70%) of the observations.

A more difficult question is: out of these katabatic-looking winds what percentage have a significant katabatic forcing? To determine this we have removed data that have a large downslope perturbation pressure gradient (presumably due to non-katabatic synoptic-scale

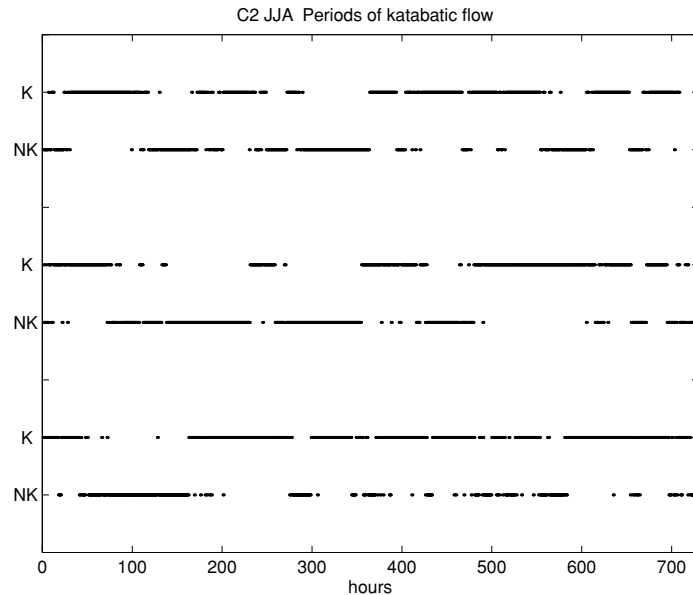


Fig. 10. An illustration of periods of katabatic (K) and non-katabatic (NK) flow for C2 during winter (JJA). The time series is wrapped around into three sections. It shows every hour as either primarily katabatic or non-katabatic as determined from wind, perturbation pressure and stability criteria. Namely, an hour is deemed katabatic if: (1) the wind speed is within 3σ and the wind direction is within 2σ of mean katabatic flow conditions (Table 6); (2) synoptic-scale influences are small (in this case $\nabla p' < 3/4$ quartile of the full JJA data set); and (3) the surface layer is unambiguously stable (in this case $\Delta\theta/\Delta z > 0.1$ K m⁻¹).

weather systems) by discarding times when $\nabla p' >$ the $3/4$ quartile of the full JJA data set; and have chosen data that are unambiguously stable (in this case choosing times when $\Delta\theta/\Delta z > 0.1$ K m⁻¹). Using these criteria 44% (or 49% if one uses the above ± 3 wind speed criteria) of the total observations at C2 and 42% (or 44%) of the total observations at C3 have katabatic forcing. This means only around 70% at C2 and 63% at C3 of the katabatic-looking winds have an unambiguous katabatic forcing. One can repeat these calculations with different definitions of katabatic-looking winds, and clearly the percentages will vary somewhat depending on the criteria chosen. However, the qualitative message is unchanged: the flow is katabatic over Coats Land 40–50% of the time, although it appears katabatic some 60–70% of the time. In other words, some considerable amount of data that appear katabatic (through their wind characteristics) are not primarily forced by a downslope buoyancy forcing.

The timing of katabatic and non-katabatic periods at C2 is illustrated as a time series in Fig. 10. Note this shows three months of hourly data wrapped into three rows for illustration purposes. Here the katabatic

data are defined (as above) - using the wind speed criteria of within ± 3 standard deviations, discarding the times when $\nabla p' >$ the $3/4$ quartile, and choosing unambiguously stable times, so the flow is katabatic 49% of the time. It is clear that there is no well defined periodicity in the surface wind regime. Katabatic periods tend to last for tens to hundreds of hours, with short interruptions (more than likely as a result of the vagaries of the katabatic selection criteria), before a switch to non-katabatic flow. A number of katabatic periods seem to last around 40–50 h. Small modifications to the katabatic selection criteria do not alter the qualitative appearance of this illustration, although we would like to stress the figure is just an illustration, not a definitive categorisation of the flow type. We would suggest that the changes illustrated here are brought about by changes in the surrounding synoptic-scale weather patterns. However, given our selection criteria are implicitly functions of the regional meteorology, we cannot prove this assertion. Indeed with the limited data set available this hypothesis is not independently testable. Our point is an illustration of changes in the flow regime at a site of ordinary katabatic winds.

6. Conclusions

A surface-based climatology of Coats Land, Antarctica, has been presented. There are clear seasonal differences, so for simplicity here we remark upon winter conditions only; although we note that these are also relevant for the equinoctial seasons. The region can be divided into two dynamical regimes: the slopes of the continent and the Brunt Ice Shelf. The continent is frequently subject to moderate katabatic winds from about 10° to the east of the fall line. Mean katabatic wind speeds are 7.5 m s^{-1} at the steepest part of the slope (at the C2 site) and 5.1 m s^{-1} higher up the slope (at the C3 site). Katabatic winds rarely exceed 15 m s^{-1} in this region; although winds stronger than this are frequent, they are associated with synoptic-scale low-pressure systems. The adjoining Brunt Ice Shelf is generally unaffected by katabatic winds, instead receiving low to moderate winds with no preferred direction during periods when the surface flow is katabatic on the continent (Fig. 9, Table 7).

The two different dynamical regimes also have a clear thermal signature. Moving up the continental slope the surface layer is generally close to constant in terms of potential temperature, but about 10 K warmer than the surface layer over the ice shelf. This scenario is most apparent for conditionally sampled clear-sky conditions, or katabatic conditions, when the surface can cool unhindered (Fig. 3, Tables 6 and 7). It would appear that the slope of the ice surface is crucial in determining the surface-layer thermal structure: where the slopes are smallest, on the ice shelf and high up the slope (at the C4 site), there is a high frequency of calm or low wind-speed conditions. Such conditions imply there is little turbulent transport of heat through the surface layer, which leads to very strong surface-layer stabilities and very low potential temperatures on the ice shelf (Table 3, Fig. 3). We would suggest that the potential temperatures high up on the slope (at C4) are not quite as low because the long-wave radiational imbalance

is smaller. On steeper slopes, calm or low wind-speed conditions are infrequent, which implies some turbulent transport of heat will be present, leading to a less-stable surface layer and higher potential temperatures.

Katabatic flows are associated with small cloud amounts and drier than average conditions, presumably due to the descent of colder air from altitude (Table 7). It is driest, in terms of relative humidity, at the steepest part of the slope. This is despite the results of a quasi-Lagrangian analysis which shows a small cooling and moistening with descent of a mean katabatic air parcel. This analysis allows estimates of the entrainment fluxes of heat and moisture, from the free atmosphere into the air parcel, of (at least) 30 W m^{-2} and (at most) 3 W m^{-2} , respectively.

The katabatic flow over the continent is modulated by large-scale weather systems which simultaneously affect all the sites. Case studies show that these are generally synoptic-scale cyclones, which have a preferential track to the north of Coats Land in the circumpolar trough (King and Turner, 1997). These cyclones bring high wind speeds, generally from the east as a result of a barrier effect from the continental slope. The high winds turbulently mix the surface layer and so homogenise the clear-sky thermal structure. A partition of the flow over the continent suggests the flow is primarily katabatic at most 40–50% of the time; although it may appear to be katabatic, in terms of wind speed and wind direction characteristics, some 60–70% of the time.

7. Acknowledgements

We thank all staff from the British Antarctic Survey who have been involved in the maintenance of the Coats Land AWSs. We also thank Russ Ladkin for help with processing the satellite imagery used in this study, and John King, Howard Roscoe, Alan Rodger and the two reviewers for useful discussions on this work.

REFERENCES

- Anderson, P. S. 1994. A method for rescaling humidity sensors at temperatures well below freezing. *J. Atmos. Ocean. Technol.* **11**, 1388–1391.
- Ball, F. K. 1960. Winds on the ice slopes of Antarctica. *Antarctic meteorology*, Pergamon Press, Oxford, 9–16.
- BAS, SPRI, and WCMC. 1993. *Antarctic digital database user's guide and reference manual*. Scientific Committee on Antarctic Research Cambridge.
- Bintanja, R. 2000. Mesoscale meteorological conditions in Dronning Maud Land, Antarctica, during summer: A qualitative analysis of forcing mechanisms. *J. Appl. Meteorol.* **39**, 2348–2370.
- Bretherton, C. S. and Pincus, R. 1995. Cloudiness and marine boundary layer dynamics in the ASTEX Lagrangian

- experiments. Part I: Synoptic setting and vertical structure. *J. Atmos. Sci.* **52**, 2707–2723.
- Bromwich, D. H. 1989a. Satellite analysis of antarctic katabatic wind behaviour. *Bull. Am. Meteorol. Soc.* **70**, 738–749.
- Bromwich, D. H. 1989b. An extraordinary katabatic wind regime at Terra Nova Bay, Antarctica. *Mon. Wea. Rev.* **117**, 688–695.
- Gallee, H. and Schayes, G. 1992. Dynamical aspects of katabatic wind evolution in the Antarctic coastal zone. *Boundary-Layer Meteorol.* **59**, 141–161.
- Gallee, H. and Pettre, P. 1998. Dynamical constraints on katabatic wind cessation in Adelie Land, Antarctica. *J. Atmos. Sci.* **55**, 1755–1770.
- Heinemann, G. 1999. The KABEG'97 field experiment: An aircraft-based study of katabatic wind dynamics over the Greenland Ice Sheet. *Boundary-Layer Meteorol.* **93**, 75–116.
- Justus, C. G., Hargreaves, W. R., Mikail, A. and Graber, D. 1978. Methods for estimating wind speed frequency distributions. *J. Appl. Meteor.* **17**, 350–353.
- King, J. C. 1993. Control of near-surface winds over an Antarctic ice shelf. *J. Geophys. Res.* **98**, 12949–12954.
- King, J. C. and Anderson, P. S. 1994. Heat and water vapour fluxes and scalar roughness lengths over an Antarctic ice shelf. *Boundary-Layer Meteorol.* **69**, 101–121.
- King, J. C. and Turner, J. 1997. *Antarctic meteorology and climatology*. Cambridge University Press, Cambridge, 409 pp.
- King, J. C. and Anderson, P. S. 1999. A humidity climatology for Halley, Antarctica, based on frost-point hygrometer measurements. *Antarctic Sci.* **11**, 100–104.
- King, J. C., Varley, M. J. and Lachlan-Cope, T. A. 1998. Using satellite thermal infrared imagery to study boundary layer structure in an Antarctic katabatic wind region. *Int. J. Remote Sensing* **19**, 3335–3348.
- King, J. C., Anderson, P. S., Smith, M. C. and Mobbs, S. D. 1996. The surface energy and mass balance at Halley, Antarctica during winter. *J. Geophys. Res.* **101**, 19119–19128.
- Kodama, Y., Wendler, G. and Ishikawa, N. 1989. The diurnal variation of the boundary layer in summer in Adelie Land, Eastern Antarctica. *J. Appl. Met.* **28**, 16–24.
- Liu, Z. and Bromwich, D. H. 1997. Dynamics of the katabatic wind confluence zone near Siple Coast, West Antarctica. *J. Appl. Met.* **36**, 97–118.
- Nakagawa, K. and Shimodoori, H. 1994. The relationship between the thermal belt on the slope of the ice sheet on the Soya coast and the surface inversion layer over Syowa station. *Proc. NIPR Symp. Polar Meteorol. Glaciol.* **8**, 53–65.
- Parish, T. R. 1988. Surface winds over the Antarctic continent: a review. *Rev. Geophys.* **26**, 169–180.
- Parish, T. R. 2001. Topographic forcing of the Antarctic wind field. *Sixth conference on Polar Meteorology and Oceanography* American Meteorological Society, San Diego, CA, 355–358.
- Parish, T. R. and Bromwich, D. H. 1987. The surface wind field over the Antarctic ice sheets. *Nature* **328**, 51–54.
- Parish, T. R. and Waight, K. T. 1987. The forcing of antarctic katabatic winds. *Mon. Wea. Rev.* **115**, 2214–2226.
- Parish, T. R. and Bromwich, D. H. 1991. Continental-scale simulation of the Antarctic katabatic wind regime. *J. Climate* **4**, 135–146.
- Parish, T. R. and Bromwich, D. H. 1998. A case study of Antarctic katabatic wind interaction with large-scale forcing. *Mon. Wea. Rev.* **126**, 199–209.
- Parish, T. R. and Cassano, J. J. 2001. Forcing of the wintertime Antarctic boundary-layer winds from the NCEP/NCAR global reanalysis. *J. Appl. Meteor.* **40**, 810–821.
- Pavia, E. G. and O'Brien, J. J. 1986. Weibull statistics of wind speed over the ocean. *J. Climate Appl. Meteorol.* **25**, 1324–1332.
- Renfrew, I. A. and Moore, G. W. K. 1999. An extreme cold air outbreak over the Labrador Sea: roll vortices and air–sea interaction. *Mon. Wea. Rev.* **127**, 2379–2394.
- Schwerdtfeger, W. 1984. *Weather and climate of the Antarctic*. Elsevier, Amsterdam, 261 pp.
- Stearns, C. R. and Weidner, G. A. 1993. Sensible and latent heat flux estimates in Antarctica. *Antarctic meteorology and climatology: studies based on automatic weather stations*. American Geophysical Union, Washington D.C., 109–138.
- Stearns, C. R., Keller, L. M., Weidner, G. A. and Sievers, M. 1993. Monthly mean climatic data for Antarctic automatic weather stations. *Antarctic meteorology and climatology: studies based on automatic weather stations*, American Geophysical Union, Washington, D.C., 1–21.
- Van den Broeke, M. R. and Van Lipzig, N. P. M. 2002. Factors controlling the near-surface wind field in Antarctica, *Mon. Wea. Rev.*, in press.
- Van den Broeke, M. R., Van Lipzig, N. P. M. and Van Meijgaard, E. 2002. Momentum budget of the East Antarctic atmospheric boundary layer: results of a regional climate model. *J. Atmos. Sci.*, in press.
- Wendler, G., Andre, J. C., Pettre, P., Gosink, J. and Parish, T. 1993. Katabatic winds in Adelie coast. *Antarctic meteorology and climatology: studies based on automatic weather stations*, American Geophysical Union, Washington, D.C., 23–46.